Lipokine 5-PAHSA Is Regulated by Adipose Triglyceride Lipase and Primes Adipocytes for De Novo Lipogenesis in Mice

Veronika Paluchova,[1] Marina Oseeva,[1] Marie Brezinova,[1] Tomas Cajka,[1] Kristina Bardova,[1] Katerina Adamcova,[1] Petr Zacek,[2] Kristyna Brejchova,[1] Laurence Balas,[3] Hana Chodounska,[4] Eva Kudova,[4] Renate Schreiber,[5] Rudolf Zechner,[5] Thierry Durand,[3] Martin Rossmeisl,[1] Nada A. Abumrad,[6] Jan Kopecky,[1] and Ondrej Kuda[1]

METABOLISM

Branched esters of palmitic acid and hydroxystearic acid (PAHSA) are anti-inflammatory and antidiabetic lipokines that connect glucose and lipid metabolism. We aimed to characterize involvement of the 5-PAHSA regioisomer in the adaptive metabolic response of white adipose tissue (WAT) to cold exposure (CE) in mice, exploring the cross talk between glucose utilization and lipid metabolism. CE promoted local production of 5- and 9-PAHSAs in WAT. Metabolic labeling of de novo lipogenesis (DNL) using ^2H_2O revealed that 5-PAHSA potentiated the effects of CE and stimulated triacylglycerol (TAG)/fatty acid (FA) cycling in WAT through impacting lipogenesis and lipolysis. Adipocyte lipolytic products were altered by 5-PAHSA through selective FA re-esterification. The impaired lipolysis in global adipose triglyceride lipase (ATGL) knockout mice reduced free PAHSA levels and uncovered a metabolite reservoir of TAG-bound PAHSAs (TAG estolides) in WAT. Utilization of ^{13}C isotope tracers and dynamic metabolomics documented that 5-PAHSA primes adipocytes for glucose metabolism in a different way from insulin, promoting DNL and impeding TAG synthesis. In summary, our data reveal new cellular and physiological mechanisms underlying the beneficial effects of 5-PAHSA and its relation to insulin action in adipocytes and independently confirm a PAHSA metabolite reservoir linked to ATGL-mediated lipolysis.

The dysregulation of both glucose and lipid metabolism in white adipose tissue (WAT) contributes to the development of obesity-associated type 2 diabetes, which represents one of the most serious health threats. However, the mechanistic links between altered glucose and lipid metabolism in the WAT of obese patients and the development of systemic insulin resistance are not fully explored. De novo lipogenesis (DNL) converts carbohydrates to energy-dense neutral lipids both in the liver and in WAT (1–4). Although hepatic DNL is usually associated with systemic insulin resistance, DNL in WAT correlates with insulin sensitivity and obesity resistance (5–8). We recently demonstrated in WAT that DNL, when combined with triacylglycerol (TAG)/fatty acid (FA) cycling activity, contributes to a lean phenotype in mice (6). This supports the notion that adipose tissue–specific regulation of DNL is critical for metabolic homeostasis (reviewed in Yilmaz et al. [4]).

DNL in WAT might also serve as a source of signaling molecules, i.e., bioactive lipids (lipokines), including palmitoleate (5), alkyl ether lipids (9), and FA esters of hydroxy FAs (FAHFAs), namely, palmitic acid hydroxystearic acids (PAHSAs) (8), molecules that promote insulin sensitivity and ameliorate insulin resistance. Structurally, FAHFAs consist of an FA (e.g., palmitic acid) esterified to a hydroxy FA (e.g., hydroxystearic acid), and the position of the branching carbon defines the regioisomer (e.g.,

---

[1]Institute of Physiology of the Czech Academy of Sciences, Prague, Czech Republic
[2]Proteomics Core Facility, Faculty of Science, Charles University, Division BIOCEV, Vestec, Czech Republic
[3]Institut des Biomolécules Max Mousseron, UMR 5247, CNRS, Université Montpellier, and Faculté de Pharmacie, ENSCM, Montpellier, France
[4]Neurosteroids, Institute of Organic Chemistry and Biochemistry of the Czech Academy of Sciences, Prague, Czech Republic
[5]Institute of Molecular Biosciences, University of Graz, Graz, Austria
[6]Department of Medicine, Washington University School of Medicine, St. Louis, MO

5-PAHSA, positional isomer). Many families of regioisomers have been identified in humans, rodents, and plants (8,10,11). The 5- and 9-PAHSA regioisomers have been the most studied for their anti-inflammatory and insulin-sensitizing effects (12,13).

During cold exposure (CE), adipose triglyceride lipase (ATGL) catalyzes TAG hydrolysis in WAT and the released FAs fuel thermogenesis in brown adipose tissue (14) while TAGs in WAT are replenished by DNL from glucose (6). Here, we explored the potential involvement of 5-PAHSA in the adaptive metabolic response of WAT to CE in mice. We tested the hypothesis that CE could associate with increased generation of PAHSA that affects both DNL and TAG/FA recycling and influences the metabolic profile of WAT.

RESEARCH DESIGN AND METHODS

Reagents
All chemical reagents were from Sigma-Aldrich (St. Louis, MO) unless stated otherwise. FAHFA standards were from Cayman Europe (Tallinn, Estonia), and 5-PAHSA (Supplementary Fig. 1) was synthesized as previously described (15). Heavy water (^2H_2O) was from CortecNET (Voisins-le-Bretonneux, France), and ^{13}C-labeled glucose and glutamine and ^2H-labeled glucose were from Cambridge Isotope Laboratories (Tewksbury, MA). TAG estolide tag 16:0/16:0/9-PAHSA [sn-3-((9-(palmitoyloxy)octadecanoyl)oxy)propane-1,2-diyldipalmitate] was synthesized from 1,2-dipalmitoyl glycerol and 9-PAHSA (Sigma) using 1-ethyl-3-(3-dimethylaminopropyl)carbodiimide and 4-dimethylaminopyridine in CH_2Cl_2.

Animal Studies
Two-month-old male B6 (C57BL/6JBomTac; Taconic Biosciences, Ejby, Denmark) mice fed standard chow were maintained close to thermoneutrality (TN) at 30°C for 1 week. Thereafter, subgroups of mice were either maintained at 30°C (control animals) or exposed to cold (CE animals) at 6°C for 7 days before killing (6). After 3 days, mice were further divided into subgroups and received an oral gavage of 5-PAHSA or saline (in a polyethylene glycol 400/TWEEN 80 formulation [8]) (Fig. 1). The 5-PAHSA dose was 45 mg/kg. EDTA plasma and various tissues were collected, including liver and epididymal WAT (eWAT). Samples were flash frozen and stored in liquid nitrogen. Global ATGL knockout (AKO) mice were generated as previously described (14). Female AKO mice and wild-type (WT) littermates fed standard chow were fasted for 12 h before dissection (fed vs. fasted state) or sacrificed at ad libitum fed state (acute and chronic CE) (14).

In Vivo Lipid Synthesis in Murine eWAT
Two days prior to dissection, mice were injected intraperitoneally with a bolus of ^2H_2O in saline (3.5 mL of 0.9% NaCl w/v in 99.9%-enriched ^2H_2O/100 g body weight) and 10% of their drinking water was replaced with ^2H_2O for the rest of the experiment to stabilize ^2H_2O content in body water as previously described (6). Deuterium enrichment of mouse plasma was assayed by exchange with acetone using GC×GC-TOFMS (two-dimensional gas chromatography time-of-flight mass spectrometry) (16). Total lipids from eWAT were extracted using the methanol/methyl tert-butyl ether/water protocol and the TAGs purified by solid-phase extraction (17,18). An aliquot of the TAG extract was hydrolyzed in KOH, the free FA converted to methyl esters, and free glycerol derivatized with N,O-bis(trimethylsilyl)trifluoroacetamide before analysis using GC×GC-TOFMS (19). The fractional synthesis of FA from ^2H_2O was calculated according to mass isotopomer analysis (20). A separate aliquot of the lipid extract was processed for lipidomics and metabolomics.

Cell Culture
3T3-L1 murine adipocytes were differentiated according to a standard protocol and mature adipocytes kept in DMEM complete medium (25 mmol/L glucose, 10% calf serum, 850 nmol/L insulin, penicillin/streptomycin) (10).

In Vitro Lipid Synthesis
3T3-L1 adipocytes were maintained in DMEM complete medium prepared from powder (D5648; Sigma-Aldrich), ^2H_2O, and water for cell cultures (50/50, v/v) (21) for 3 days. Total lipids were extracted as above and processed for lipidomics, and the raw data were analyzed with MS-DIAL version 2.52 software (22). Data from labeling experiments (^{13}C and ^2H) were adjusted for C, H, and O natural abundance and tracer purity using IsoCor 2.0.5 (23), and the fractional synthesis of intact lipids was estimated according to the mass isotopomer analysis (20,24). Parallel reaction monitoring and tandem mass spectrometry (MS/MS) scanning modes of the Q Exactive Plus mass spectrometer (Thermo Fisher Scientific, Bremen, Germany) were used to confirm M+3 isotopologue identity and glycerol backbone labeling.

Glucose Uptake and PAHSA Treatment
Mature 3T3-L1 adipocytes were grown in full DMEM for 3 days in the absence or presence of 5-PAHSA, similar to the duration of 5-PAHSA gavage in mice. Adipocytes were serum starved in DMEM with 0.1% (w/v) BSA for 15 h, washed, and kept in DMEM without glucose and glutamine (A1443001; Gibco) for 30 min. Cells were then labeled with $^{13}C_6$-glucose (5.5 mmol/L in A144301 medium) in the presence or absence of 40 μmol/L 5-PAHSA for 0, 5, 10, and 15 min in a reverse time course fashion, similar to that described by Krycer et al. (25). Metabolism was quenched in a water bath (0°C), and cells were washed twice with ice-cold PBS, lysed in the methanol/water fraction of the methyl tert-butyl ether extraction mixture chilled at −20°C, and frozen in liquid nitrogen. Alternatively, cells were preincubated with 10 nmol/L insulin in the glucose-free media and labeled with $^{13}C_6$-glucose (5.5 mmol/L final) with or without 10 nmol/L insulin, and the metabolism was quenched after 10 min.
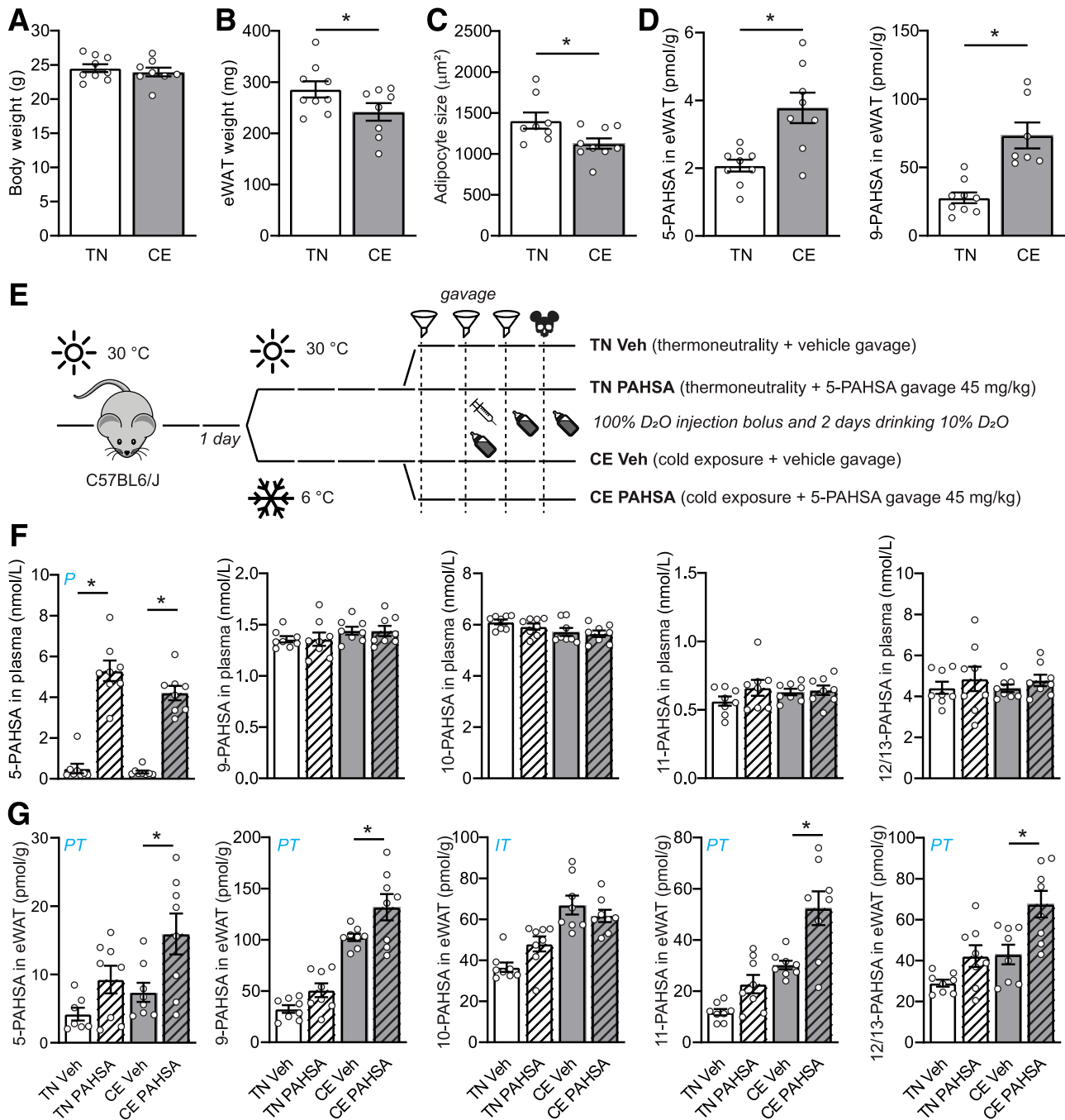
Figure 1—PAHSA levels were increased in cold. *A*: Body weight of male C57BL/6J mice maintained at TN (30°C) and then either kept at TN or exposed to cold (6°C) for 7 days. *B*: Weight of eWAT. *C*: Size of adipocytes in eWAT. *D*: Concentration of 5- and 9-PAHSA in eWAT. Data are means ± SEM (*n* = 8–9). *P < 0.05 by Student *t* test. *E*: Experiment combining TN, CE, gavage of 5-PAHSA, and deuterium metabolic labeling. *F*: Levels of PAHSA regioisomers in plasma. *G*: Levels of PAHSA regioisomers in eWAT. Two-way ANOVA with multiple comparison test (Sidak) was used. Letters within the graphs denote a statistically significant effect of 5-PAHSA (*P*), temperature (*T*), or interaction of factors (*I*). Data are means ± SEM (*n* = 8–9). *Planned multiple comparison of the effect of 5-PAHSA at the given temperature statistically different at *P* < 0.05. D₂O, heavy water; Veh, vehicle.

To explore the contribution of glutamine carbons, the labeling media were supplemented with 5.5 mmol/L glucose and 4 mmol/L $^{13}C_5$-glutamine, and the metabolism was quenched after 10 min of glucose uptake.

FAHFA Analysis

Plasma, eWAT, cells, and media were processed according to published methods (10,18) with special attention paid to known methodological issues (26,27).

Metabolomics, Lipidomics, Bioinformatics, and Statistical Analyses

The liquid chromatography (LC)-MS system consisted of a Vanquish UHPLC System (Thermo Fisher Scientific) coupled to a Q Exactive Plus mass spectrometer. See Supplementary Data for details.

LC-MS and LC-MS/MS data were processed through the software MS-DIAL, version 2.52 (22), using its isotope tracking features. Metabolites were annotated using an in-house retention time charge/mass ratio (*m/z*) library and using MS/MS libraries available from public sources (MassBank of North America [MoNA]). Normalized (locally estimated scatterplot smoothing procedure, Python script) peak heights/data from labeling experiments (^{13}C and ^2H) were adjusted for C, H, and O natural abundance and tracer purity using IsoCor 2.0.5 (23) when needed. An in silico library of theoretical TAG estolides was calculated using EnviPat (28) and in-house Python scripts. GraphPad Prism 8.0.2 software was used to compare groups (Student *t* test, ANOVA, etc.).

Data and Resource Availability

The data sets generated and/or analyzed during the current study are available from the corresponding author upon reasonable request. No applicable resources were generated or analyzed during the current study.

RESULTS

PAHSA Levels Are Increased by CE

We previously showed that induction of DNL in WAT during CE was associated with a lean phenotype in mice (6). To explore the involvement of PAHSAs in this metabolic adaptation, we examined mice kept at TN or exposed to cold for 7 days. In response to CE, body weight was not affected, while the weight of eWAT and adipocyte size decreased (Fig. 1A–C), similar to previous studies (6,29). Levels of both 5- and 9-PAHSA in eWAT were elevated by CE (Fig. 1D). Therefore, we explored the effect of 5-PAHSA, administered by gavage for 3 days, on DNL in eWAT of mice kept either at TN or exposed to cold for 7 days. In these studies heavy water (^2H_2O) was used as a tracer for lipogenesis (Fig. 1E). The 5-PAHSA gavage led to an approximately fivefold increase in plasma 5-PAHSA levels with no changes in other PAHSA regioisomers at either TN or cold temperature (Fig. 1F). Intriguingly, we noticed that the levels of nearly all PAHSA regioisomers were increased in eWAT after 5-PAHSA gavage, especially in CE animals (Fig. 1G), suggesting a modulation of DNL. Of note, the
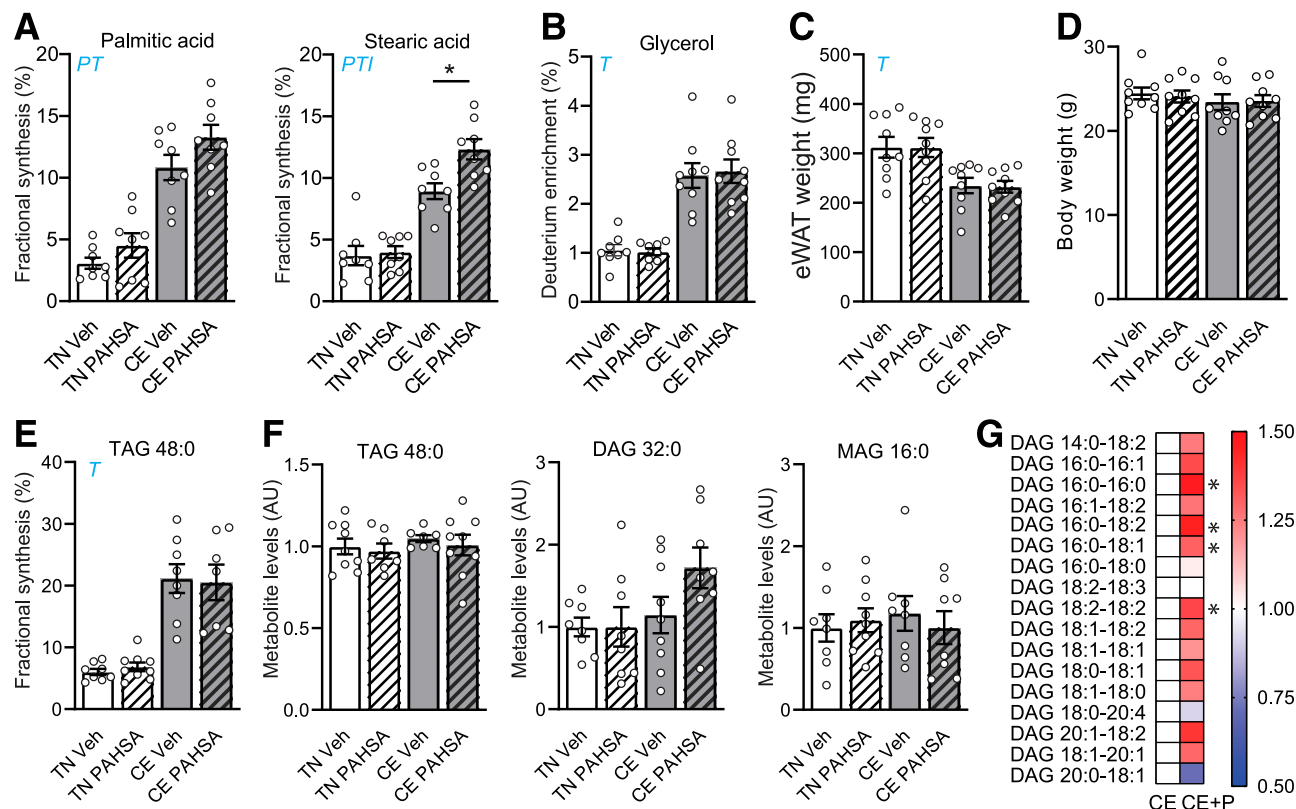
Figure 2—5-PAHSA stimulated DNL in eWAT during CE. *A*: Fractional synthesis of palmitic and stearic acid measured in hydrolysates of the TAG fraction of eWAT (see experiment in Fig. 1E). Two-way ANOVA with multiple comparison test (Sidak) was used. Letters within the graphs denote a statistically significant effect of 5-PAHSA (*P*), temperature (*T*), or interaction of factors (*I*). *Planned multiple comparison of the effect of 5-PAHSA at the given temperature statistically different at $P < 0.05$. *B*: Deuterium enrichment of glycerol measured in hydrolysates as above. *C*: Weight of eWAT. *D*: Body weight of animals. *E*: Fractional synthesis of TAG 48:0 (TAG 16:0_16:0_16:0). *F*: Relative levels of TAG 48:0, DAG 32:0 (16:0_16:0), and MAG 16:0. *G*: Profile of DAGs comparing CE and CE 5-PAHSA (CE + P) groups. Data are means ± SEM. *$P < 0.05$ by Student *t* test (*n* = 8–9). AU, arbitrary units; Veh, vehicle.

concentration and ionization efficiency of 5-PAHSA is lower compared with other PAHSAs. Therefore, the variations between experiments are larger than for other PAHSA regioisomers.

5-PAHSA Stimulates DNL and Lipid Remodeling in eWAT During CE

We took advantage of the in vivo deuterium labeling of cellular lipids in both TN and CE mice (see above) and analyzed (gas chromatography–mass spectrometry) the deuterium enrichment of *1*) FAs liberated by hydrolysis of eWAT lipid extract and *2*) plasma water to calculate the fractional rate of palmitate and stearate synthesis (Fig. 2*A*). The palmitate synthesis data showed a clear uptrend in both TN and CE mice, while the stearate data showed that 5-PAHSA stimulated DNL in the CE mice but not in the TN mice. Glycerol deuterium enrichment (Fig. 2*B*) and eWAT weight (Fig. 2*C*) were only affected by CE and not by 5-PAHSA treatment, indicating an effect independent of glyceroneogenesis. In addition, body weight was unaffected (Fig. 2*D*), leading us to conclude that the 5-PAHSA stimulation of DNL promoted not lipid storage but, rather, a form of energy-consuming DNL and TAG/FA remodeling.

We then performed a lipidomic analysis of deuterium-labeled intact lipids extracted from eWAT using LC-MS. Many lipid species were found to be enriched with deuterium, but the TAGs with shorter-chain FAs, especially TAG 16:0_16:0_16:0 (TAG 48:0) and 16:0_16:0_16:1 (TAG 48:1), were the most labeled species. In the CE mice, the fractional synthesis of TAG 48:0 was significantly higher than with the TN mice (Fig. 2*E*). The absolute levels of TAG 48:0 were similar in all the groups, but the levels of diacylglycerol (DAG) 16:0_16:0 (DAG 32:0), the lipolytic product of TAG 48:0, tended to be higher in the CE PAHSA group, while there was no difference in mono-acylglycerol (MAG) 16:0 levels (Fig. 2*F*). The same pattern applied to TAG 48:1 (Supplementary Fig. 2*A*). Detailed analysis of DAG levels in the CE animals showed that 5-PAHSA induced a global increase in acylglycerol remodeling (Fig. 2*G* and Supplementary Fig. 2*B*).

FAHFAs Are Liberated From TAG Estolides During Lipolysis via ATGL

Yore et al. (8) reported the puzzling findings that levels of PAHSA increased during fasting while being associated with DNL during refeeding. Here, we observed that PAHSA levels were also elevated during CE when eWAT metabolism balances lipolysis and lipogenesis. Moreover, when we tried to measure PAHSA synthesis using the ^2H_2O approach during fasting in mice, we were unable to detect any deuterium enrichment of PAHSAs. This observation suggests that PAHSAs were released from a specific cellular pool during lipolysis. We hypothesized that the best chemical form for FAHFA storage would be a TAG estolide, a TAG-like molecule containing esterified FAHFA (30). To test this, we analyzed mouse eWAT lipid extracts and focused our LC-MS/MS measurement on the higher m/z

range. Indeed, we found several analytes matching our in silico library and were able to identify them by the number of carbons and double bonds (Table 1). The structure of TAG estolide 16:0_18:2_18:0-(O-16:0) and the minor components containing 16:0/18:0/18:1/18:2 and -(O-18:1) acyls was assigned based on the structure and fragmentation patterns of a synthetic standard (Fig. 3*A* and *B* and Supplementary Fig. 3). It was identical to a recently reported PAHSA-containing TAG species (31). Several coeluting analytes were identified as FAHFA-containing TAG estolides, but further method development will be needed for detailed structural analysis including the position of acyl chains and hydroxy FA branching carbon of the isomers. We hypothesized that the FAHFAs might be released via lipolysis. When 3T3-L1 adipocytes differentiated in vitro were stimulated with forskolin, free FAHFA levels increased, while the ATGL inhibitor atglistatin (32) prevented the release of glycerol, FAs, and FAHFAs (Fig. 3*C*). Therefore, we explored this further using eWAT of ATGL-deficient (AKO) mice in the fed and fasted state (Fig. 3*D*). Interestingly, TAG estolides were higher in the fasted than in the fed state in WT animals, while this regulation was absent in the AKO mice and also the TAG EST levels were minimal in the AKO mice. Furthermore, the levels of free 5- and 9-PAHSA followed the same pattern (Fig. 3*E*). We also analyzed

Table 1—List of TAG estolides containing an FAHFA regioisomer detected in mouse eWAT

RT (min)	*m/z*	ID
5.67	1,126.9990	TAG EST 68:4
5.83	1,129.0135	TAG EST 68:3
5.96	1,131.0292	TAG EST 68:2
5.68	1,153.0143	TAG EST 70:5
5.84	1,155.0234	TAG EST 70:4
5.95	1,157.0442	TAG EST 70:3
5.83	1,157.0435	TAG EST 70:3
5.97	1,159.0581	TAG EST 70:2
5.68	1,179.0291	TAG EST 72:6
5.81	1,181.0447	TAG EST 72:5
5.94	1,183.0615	TAG EST 72:4
5.69	1,181.0448	TAG EST 72:5
5.83	1,183.0594	TAG EST 72:4
5.96	1,185.0747	TAG EST 72:3
6.01	1,187.0918	TAG EST 72:2
5.66	1,205.0460	TAG EST 74:7
5.69	1,207.0609	TAG EST 74:6
5.82	1,209.0753	TAG EST 74:5
5.95	1,211.0929	TAG EST 74:4

Identification is based on the number of carbons and double bonds, *m/z* as ammonium adducts $[M + NH_4]^+$, retention time (RT), MS/MS spectra, and fragmentation patterns of the synthetic standard TAG EST 16:0/16:0/9-PAHSA. EST, estolide; ID, identifier.
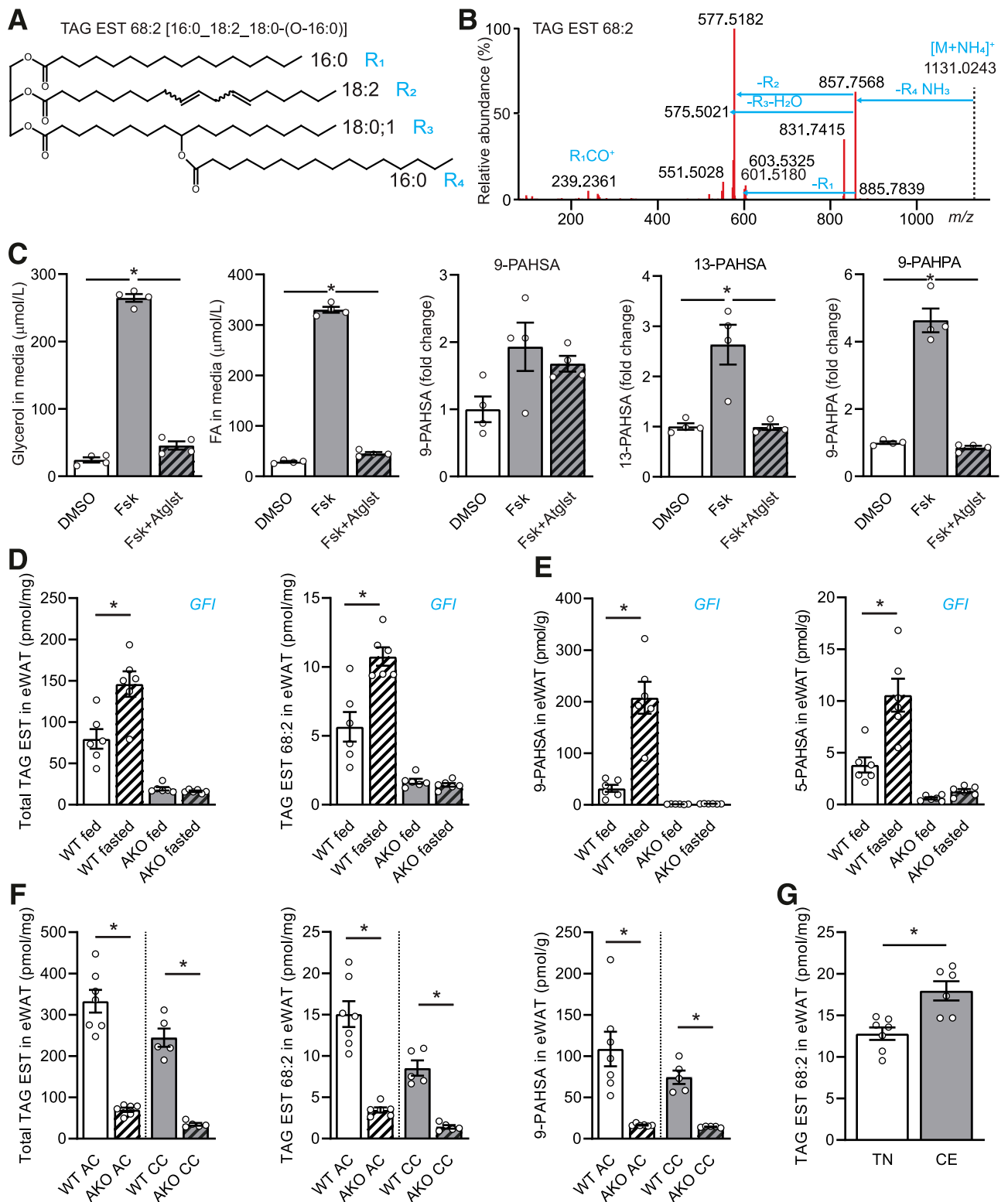
Figure 3—FAHFAs are liberated from TAG estolides during lipolysis. *A*: Tentative structure of a TAG estolide containing 9-PAHSA. This structure was deduced from MS/MS spectra observed in eWAT mouse extracts. The technique does not allow us to assign acyl position, double-bond position, and geometry. *B*: MS/MS spectrum of the measured analyte (see Supplementary Fig. 3 for annotations). *C*: 3T3-L1 adipocytes were preincubated with or without atglistatin (Atglst) and stimulated with forskolin (Fsk) for 2 h, and levels of glycerol and free FAs were determined in the media. Cells and media were extracted, and levels of free FAHFAs were measured using LC-MS/MS. DMSO indicates control cells incubated with DMSO. Data are means ± SEM ($n = 4$). One-way ANOVA with multiple comparison test (Dunnett) was used to compare means with the mean of the Fsk group. *Statistically different at $P < 0.05$. *D*: eWAT samples from WT and AKO mice were harvested in the fed and fasted state and analyzed using LC-MS/MS. Levels of TAG estolides containing PAHSAs (TAG EST 68:2 as a representative) and total levels of TAG EST are shown. *E*: Levels of free 9-PAHSA and 5-PAHSA in eWAT of WT and AKO mice analyzed in the same extract

TAG estolides and 9-PAHSA in WT and AKO animals exposed to acute cold (6 h) and chronic cold adaptation (3 weeks) (14) (Fig. 3F) as well as in TN and CE mice (Fig. 3G). Acute cold increased total levels of TAG estolides above those in the fasting state, and levels remained high in cold-adapted WT animals. In AKO mice, total TAG estolide levels slightly increased in response to cold, but values were much lower compared with WT mice (Fig. 3F). A difference in the changes in total TAG estolide levels, TAG estolide 68:2, and 9-PAHSA (as the representatives of all isomers) suggested that free FAHFA levels were increased through ATGL-mediated release from TAG estolides and that multiple levels of substrate specificity are involved.

5-PAHSA Modulates Both Lipogenesis and Lipolysis

Not all DAGs were affected the same way by 5-PAHSA (Fig. 2G), so we investigated whether there was an FA-specific metabolic pattern. Differentiated 3T3-L1 adipocytes were grown in a culture medium containing 50% ^2H_2O for 3 days with or without 5-PAHSA. The deuterium enrichment of TAGs showed that 5-PAHSA–treated cells incorporated more deuteria into shorter and saturated/monounsaturated "nascent" TAGs (Fig. 4A), but there were also differences in the position of incorporated deuteria within the molecule. Both the TAG acyl chains and the glycerol backbone can be labeled with deuterium through different pathways (33). We observed that TAG 48:0 was labeled mainly on the acyl chains (produced through DNL) and not as the M+3 isotopologue, which represents the TAG glycerol backbone labeled during glycolysis (Fig. 4B and Supplementary Fig. 4 for MS/MS spectra explanation).

Both lipolysis and FA esterification contribute to eWAT lipid metabolism during CE, balancing effects of catecholamines and insulin. Catecholamines stimulate release of FAs from WAT to supply brown adipose tissue heat production. The mice had access to food and therefore, in parallel, insulin stimulated glucose uptake into WAT to promote DNL and the TAG/FA cycle to buffer lipolysis. We examined the effect of 5-PAHSA on both pathways. 3T3-L1 adipocytes were grown with or without 5-PAHSA for 3 days, serum starved, preincubated with 10 nmol/L insulin or 5-PAHSA for 30 min, and subsequently exposed to forskolin for 2 h. Glycerol release into the medium showed that insulin partially countered lipolysis but 5-PAHSA slightly enhanced the effect of forskolin. Release of FAs was completely inhibited by insulin, while the effect of 5-PAHSA was not significant (Fig. 4C). Similar effects were observed with acute 5-PAHSA stimulation and isoproterenol on cultured and freshly isolated adipocytes (Supplementary Fig. 4E and F). Both markers of lipolysis suggested that 5-PAHSA affects FA re-esterification. Detailed analysis of media FA composition revealed a strong effect of 5-PAHSA on re-esterification of monounsaturated FA, especially 16:1 (i.e., palmitoleic acid), while the predominant FAs in TAGs (16:0, 18:1) accounted for net lipolysis (Fig. 4D). This effect was not observed using an acute preincubation with 5-PAHSA (Supplementary Fig. 4G). Furthermore, we tested the effect of combination of 5-PAHSA and insulin on isoproterenol-stimulated 3T3-L1 adipocytes (34) and found that 5-PAHSA stimulated glycerol release and counteracted insulin action (Fig. 4E). We conclude that 5-PAHSA significantly increased glycerol release and influenced FA release and re-esterification.

We added a $^{13}C_6$-glucose tracer in the forskolin experiment to explore metabolite labeling in the cells. We found that both insulin and 5-PAHSA prevented the decline during lipolysis of TAG 48:1, which proved to be a sensitive marker of DNL and lipid remodeling with the FA 16:1 (Fig. 4F). The M+3 isotopologue of TAG 48:1, corresponding to ^{13}C labeling of the glycerol backbone provided by glycolysis (Fig. 4F and Supplementary Fig. 4), proved that insulin drove glucose to the FA esterification pathway. In contrast, the levels of DAG 32:1, the lipolytic product of TAG 48:1, were higher in 5-PAHSA–treated cells, again pointing to TAG remodeling. Interestingly, the ^{13}C-labeling profile of citrate and its levels suggested that in contrast to insulin, 5-PAHSA directs glucose carbons to DNL instead of the glycerol backbone for esterification to TAGs (Fig. 4F).

5-PAHSA Primes Adipocytes for Glucose Metabolism and DNL

We next performed a glucose uptake experiment using $^{13}C_6$-glucose as a tracer and a major carbon source. Serum-starved 3T3-L1 adipocytes were preincubated with or without 5-PAHSA for 30 min, and then the metabolism of $^{13}C_6$-glucose was monitored for 0, 5, 10, and 15 min. The metabolites that were positively or negatively affected by 5-PAHSA are highlighted in green and red, respectively, in Fig. 5A. The levels of glucose and hexose 6-phosphates, which estimate glucose uptake, were higher in 5-PAHSA–treated cells, in agreement with previous data (8). 5-PAHSA stimulated ^{13}C enrichment and exchange of three carbon units within the lower part of the pentose phosphate pathway and glycolysis (Fig. 5B). In contrast, levels and labeling of

as above. Data are means ± SEM (n = 6). Two-way ANOVA with multiple comparison test (Tukey) was used. Letters in the graphs denote statistically significant effect of genotype (G), feeding status (F), or interaction of factors (I). *Multiple comparison of the effect of the condition with the given genotype statistically different at $P < 0.05$. Additional statistics are presented in Supplementary Table 1 for clarity. F: eWAT samples from WT and AKO mice were harvested in the fed state after acute cold (AC) (3 h) and chronic cold (CC) (3 weeks) and analyzed using LC-MS/MS. Levels of TAG estolides containing PAHSAs (TAG EST 68:2 as a representative), total levels of TAG EST, and levels of free 9-PAHSA are shown. Data are means ± SEM (n = 5–7). *$P < 0.05$ by Student t test. Vertical line separates AC and CC experiments. G: Levels of TAG EST 68:2 in eWAT samples from WT mice kept at TN or exposed to cold for 7 days as in Fig. 1. Data are means ± SEM (n = 6–7). *$P < 0.05$ by Student t test. EST, estolide.
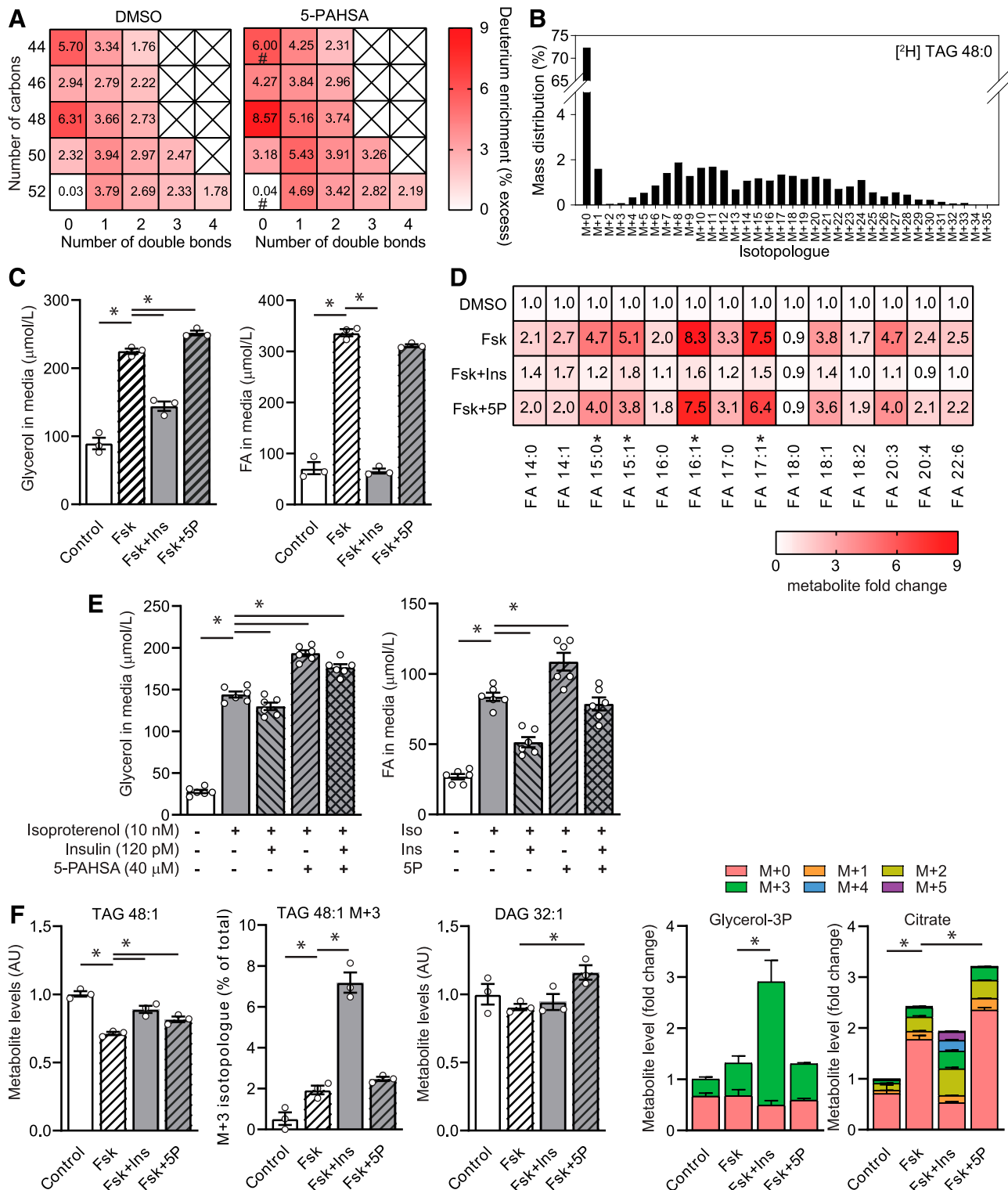
Figure 4—5-PAHSA–stimulated lipogenesis and selectively modulated lipolysis. *A*: 3T3-L1 adipocytes were grown in the presence or absence of 40 μmol/L 5-PAHSA for 3 days and labeled with 50% ^{2}H$_2$O. The deuterium enrichment of intact TAG molecules, marking the rate of lipogenesis, was measured using LC-MS/MS and is expressed as a heat map of TAGs sorted according to the number of carbons and double bonds. All fields were significantly different at $P < 0.05$ (Student *t* test, DMSO vs. 5-PAHSA) except for those marked with #, where the numbers in the fields are means ($n = 6$). *B*: Illustrative profile of deuterium-labeled TAG 48:0. *C*: Lipolysis: 3T3-L1 adipocytes were preincubated with insulin (Ins) or 40 μmol/L 5-PAHSA (5P) and stimulated with 1 μmol/L forskolin (Fsk). Glycerol and free FAs in media were measured using colorimetric kits. One-way ANOVA with multiple comparison test (Dunnett) comparing means with the mean of the Fsk group was used. Data are means ± SEM ($n = 3$). *Statistically different at $P < 0.05$. *D*: Lipolysis: levels of individual FAs in media were measured using LC-MS/MS; numbers in the fields are means ($n = 8$–9). *Statistically different at $P < 0.05$ by one-way ANOVA as above. *E*: Lipolysis: 3T3-L1 adipocytes were preincubated with 120 pmol/L Ins, 40 μmol/L 5P, or their combination and stimulated with 10 nmol/L isoproterenol

glycerol-3-phosphate were reduced by 5-PAHSA, consistent with the lipid-labeling data of Fig. 4. 5-PAHSA also channeled glucose carbons to the Krebs cycle through both pyruvate dehydrogenase and pyruvate carboxylase rather than to lactate. This was similar to the effect of insulin pretreatment on adipocytes, which primed metabolism for lipid synthesis and NADPH production through malate-pyruvate recycling (25). [4-^{2}H]glucose as a malic enzyme tracer confirmed that 5-PAHSA treatment significantly increased the ^{2}H-labeled fraction of cytosolic NADPH compared with control cells (Supplementary Fig. 5). The intermediates of the Krebs cycle decreased over time, probably due to of absence of glutamine in the medium and to lack of related anaplerotic reactions.

We then repeated the uptake experiment to test the effect of 10 nmol/L insulin (Fig. 5C) and quenched metabolism after 10 min, when the differences were maximal. Although insulin was a much stronger stimulant of glucose metabolism than 5-PAHSA, the specific 5-PAHSA pattern of three-carbon-unit metabolism was preserved. 5-PAHSA diverted carbon flux from glycerol-3-phosphate and rapid FA esterification downstream to the Krebs cycle.

Adipocytes use several carbon sources to supply the demands of DNL, and glutamine is an important player. Therefore, we repeated the glucose uptake experiment in the presence of 5.5 mmol/L glucose and 4 mmol/L ^{13}C$_5$-glutamine and quenched metabolism after 10 min. When supply of major carbon sources was not limited, 5-PAHSA–treated adipocytes used significantly more carbon from glutamine (Fig. 6A). Interestingly, ^{13}C$_5$-glutamine was metabolized both into succinate (M+4 labeling) and into M+5 citrate by reductive carboxylation, in good agreement with previously reported results (35) (Fig. 6B and C).

The above-described effects of 5-PAHSA on adipocyte metabolism are summarized in the scheme of Fig. 6D. While insulin (in red) stimulates glucose uptake and the utilization of glycerol-3-phosphate for rapid TAG synthesis, 5-PAHSA (in green) supports a longer, more energy-consuming path that involves DNL and TAG remodeling.

DISCUSSION

Here we demonstrate that 5-PAHSA, a lipokine with beneficial metabolic effects, primes adipocytes for glucose utilization and DNL while enhancing metabolically specific TAG/FA cycling. We used a combination of mouse experiments with metabolic labeling of lipogenesis and lipolysis together with dynamic metabolomics in cultured adipocytes to explore the pathways connecting glucose and lipid metabolism.

The energy-consuming combinations of TAG/FA cycling and DNL in adipocytes represent key components of a metabolically "healthy adipocyte" and are induced by CE (6,36). Our initial observation that CE increased PAHSA levels in eWAT suggested that these lipokines and DNL could be the mechanistic link underlying the metabolic changes. The experiment with 5-PAHSA oral gavage in mice at two housing temperatures with deuterium labeling of lipid synthesis proved that the effect of 5-PAHSA at TN is minimal, while CE is associated with higher PAHSA levels in eWAT. In addition, 5-PAHSA gavage increased levels of other PAHSA regioisomers in eWAT.

5-PAHSA stimulated DNL beyond the effect of CE, but it did not potentiate FA re-esterification with glucose-derived glycerol (direct TAG synthesis, fat accumulation). There was limited deuterium incorporation (only up to four deuteria) into palmitic and stearic acids in CE mice. Therefore, the effect observed at the level of FA hydrolyzed from TAGs was not clear at the level of intact lipids, where the deuterium tracer was diluted among all TAG FA combinations and insufficient tracer sensitivity was a limitation. Total metabolite level analysis suggested that 5-PAHSA affected lipid remodeling between TAGs and DAGs. The simplest interpretation is that 5-PAHSA stimulated de novo lipid synthesis from acetyl-CoA and acylglycerol remodeling, inducing a futile TAG/FA cycle that did not support lipid storage. In line with this, no effect on body weight was observed in mice chronically treated with PAHSAs (37). Our data suggest that two concurrent overlapping mechanisms were stimulated: 1) futile (energy wasting) TAG/FA cycling (6), which builds and breaks TAG completely, and 2) lipid remodeling of the TAG acyls, including FAHFAs and TAG estolides. Therefore, with respect to the metabolic rearrangements that are associated with obesity, 5-PAHSA positively affects adipocyte metabolism.

FAHFA levels rise during CE and with fasting in mice and rats (8,18). Because we were unable to detect any deuterium-labeled PAHSAs in either CE animals or fasted/refed mice, we looked for a metabolic storage pool from which PAHSA would be liberated during stimulated lipolysis. Using lipidomic profiling, we were able to identify several members of the TAG estolide lipid class in which PAHSAs are esterified to the glycerol backbone alongside two other acyl chains. The structural patterns were confirmed using a synthetic standard. We estimate that there are dozens of TAG estolides that contain other FAHFAs, but a targeted analytical approach using multistage fragmentation (MS^4) will be needed to explore their complexity. It is difficult to separate all FAHFA regioisomers, and

---

(Iso). Glycerol and free FA in media were measured using colorimetric kits. One-way ANOVA with multiple comparison test (Dunnett) comparing means with the mean of the Iso-alone group was used. Data are means ± SEM (*n* = 6). *Statistically different at *P* < 0.05. *F*: Lipolysis: levels of metabolites related to TAG 48:1 (16:0_16:0_16:1) were measured in the harvested cells using LC-MS/MS. ^{13}C$_6$-glucose was used as a tracer and citrate as a precursor of DNL. Data are means ± SEM (*n* = 3). *Statistically different at *P* < 0.05 by one-way ANOVA as above. AC, acute CE; AU, arbitrary unit; CC, chronic CE; Glycerol-3P, glycerol 3-phosphate.

Figure 5—5-PAHSA primes adipocytes for glucose (Glc) utilization toward DNL and away from FA esterification. *A*: Glc uptake. Schematic representation of the metabolic pathways affected by 5-PAHSA treatment. Statistically significant differences between DMSO and 5-PAHSA treatments are highlighted in green (upregulation) and red (downregulation) (see below). Major pathways are labeled in blue. See Supplementary Table 2 for abbreviations of the metabolites. Once Glc enters the cell and is phosphorylated, the majority of the G6P is metabolized through glycolysis to three carbon units (e.g., GAP), but some Glc molecules are processed through ancillary pathways (e.g., the pentose phosphate pathway, glycogen synthetic pathway, lipid synthesis). GAP can be further metabolized to Pyr through the lower glycolysis pathway and converted to Lac or oxidized in the Krebs cycle. Mitochondrial Cit can be exported to the cytosol and serve as a substrate for DNL, while Pyr-Mal recycling generates NADPH to fuel the DNL. *B*: Glc uptake (UGlc): time profiles of isotopologues of selected metabolites. $^{13}C_6$-Glc uptake was measured in serum-starved 3T3-L1 adipocytes preincubated without DMSO or 5-PAHSA (40 μmol/L), and the metabolism was quenched at specific time points (0, 5, 10, and 15 min). Whole bars indicate means ± SEM of the total metabolite levels, and individual isotopologues are colored according to the key (n = 3). Glc was the only major source of carbons. Two-way repeated-measures ANOVA with Sidak multiple comparison test was performed on total metabolite levels: *statistically significant difference between DMSO and 5-PAHSA at the specific time point, #statistically significant interaction between time and treatment; additional statistics are presented in Supplementary Table 2 for clarity. *C*: Glc uptake: the same experiment was repeated with or without insulin (10 nmol/L), and cell metabolism was quenched at 10 min (n = 6). Whole bars indicate means ± SEM of the total metabolite levels, and individual isotopologues are colored according to the key (n = 6). Two-way ANOVA with Tukey multiple comparison test was performed on total metabolite levels: *Statistically significant difference between DMSO and 5-PAHSA in combination with insulin. For clarity, additional statistics are presented in Supplementary Table 3. D, DMSO; D+I, DMSO and insulin; P, 5-PAHSA; P+I, 5-PAHSA and insulin.

separation and structural analysis of low-abundance TAG estolides is at the edge of current technological limits. Our data are in agreement with and confirm those recently reported on FAHFA TAGs (identical to TAG estolides) (31).

Liberation of FAHFAs from TAG estolides during lipolysis and fasting/CE was prevented by inhibition or absence of ATGL. The FAHFA increase during fasting/CE is linked to the lipolytic activity of ATGL or hormone-sensitive lipase (31). Low levels of TAG estolides in AKO mice suggest that ATGL might also be involved in their metabolism via acyltransferase activity (38,39), independent of acyl CoA:DAG acyltransferases (31). The effect of atglistatin on forskolin-treated adipocytes was more pronounced on free FAHFA levels, and TAG estolides were not changed during this short incubation (data not shown), further

Figure 6—5-PAHSA promotes glutamine (Gln) utilization for DNL. *A*: Glucose (Glc) uptake II was measured in serum-starved 3T3-L1 adipocytes preincubated with or without 5-PAHSA (40 μmol/L), and metabolism was quenched at 10 min. $^{13}C_5$-Gln (4 mmol/L) was used as a tracer. Levels of traced metabolites and their isotopologue profiles are colored according to the key. Bars indicate means ± SEM of the total metabolite levels. *B*: Glc uptake II: ^{13}C-labeled intermediates of Krebs cycle, succinate (Suc), and citrate (Cit), illustrating the fate of Gln carbons. Data are means ± SEM ($n = 5$). *$P < 0.05$ by Student t test. *C*: Atom transition map depicting a model of carbon labeling within the first turn of the Krebs cycle. $^{13}C_5$-Gln carbons enter the Krebs cycle as α-ketoglutarate (aKG), produce $^{13}C_4$-Suc (Suc M+4 [as in *B*]), and label lipids (green path). Alternatively, Cit M+5 (as in *B*) is formed through a reductive carboxylation process. *D*: Metabolic scheme summarizing metabolite labeling data and the effects of 5-PAHSA. Dotted lines represent a sequence of reactions. ACoA, acetyl-CoA; LPA, lysophosphatidic acid; MCoA, malonyl-CoA; Oxa, oxaloacetate. See Supplementary Table 2 for abbreviations of the other metabolites.

supporting a dual role of ATGL in FAHFA metabolism. The new role of ATGL in controlling the release of FAHFAs from TAG estolide stores in adipocytes, together

with the stimulation of TAG/FA remodeling by FAHFAs that we describe, is compatible with the previously unexplained observation that ATGL is required for

stimulation of DNL, TAG/FA cycling, and mitochondrial electron transport by the β3-adrenergic pathway in adipose tissue (29). Innovative lipidomic analyses capable of quantifying individual TAG estolides and FAHFA isomers will be needed to explore substrate specificity of ATGL and its contribution to FAHFA metabolism.

A study of lipogenesis and lipolysis in 3T3-L1 adipocytes showed that the prolipogenic effect of 5-PAHSA is significant but does not promote excess lipid storage, in agreement with previous data (40). Newly synthesized short FAs are primarily incorporated into short-chain TAGs, probably on the surface of small lipid droplets, allowing high turnover. Intriguingly, although the effect of 5-PAHSA on net lipolysis was mild, the selective re-esterification of monounsaturated FAs highlighted fine-tuning of the TAG/FA remodeling cycle and the ability of 5-PAHSA to spare or rebuild specific TAGs, possibly also TAG estolides.

A comparison with the effect of insulin using the ^{13}C-tracer data, specifically involving the labeling pattern of glycerol-3-phosphate and citrate, prompted us to thoroughly explore the glucose utilization pathway. Dynamic metabolomic profiling of 3T3-L1 adipocytes preincubated with insulin showed how cells select specific metabolic pathways to optimize metabolic flux and secure NADPH-producing reactions for DNL (25). We performed an analogous experiment with 5-PAHSA preincubation and found that the lipokine activated similar pathways, with an important difference in the fate of glucose carbons. In contrast to insulin, 5-PAHSA specifically reduced carbon flux to glycerol-3-phosphate, away from TAG accumulation, while enhancing carbon flux to the Krebs cycle and DNL precursors. Although the effect of 5-PAHSA was small compared with the net effect of insulin, the critical metabolic pattern was observed even when both 5-PAHSA and insulin were present. The combination of insulin and PAHSA could potentially be used therapeutically in metabolic situations where glycolysis is dysregulated.

In contrast to Krycer et al. (25), we performed the labeling experiment in media with limited carbon sources to unmask 5-PAHSA effects. The addition of glutamine, which is an important lipogenic source in adipocytes, revealed that the flux toward DNL might be even higher when the Krebs cycle can use anaplerotic substrates. This alternative fate of glucose carbons might lower fat accumulation in WAT and contribute to other antidiabetic effects of PAHSAs (8).

In summary, we propose that FAHFAs are synthesized via DNL through hydroxylated intermediates (18) and stored as TAG estolides in lipid droplets. ATGL-mediated lipolysis releases free FAHFAs, which limit FA esterification into TAG while promoting TAG acylglycerol remodeling and the fine-tuning of lipolysis. These effects prime adipocytes for glucose metabolism, in a different way from insulin, once it becomes available, and promote metabolically "healthy adipose tissue."

References

1. Eissing L, Scherer T, Tödter K, et al. De novo lipogenesis in human fat and liver is linked to ChREBP-β and metabolic health. Nat Commun 2013;4:1528
2. Solinas G, Borén J, Dulloo AG. De novo lipogenesis in metabolic homeostasis: more friend than foe? Mol Metab 2015;4:367–377
3. Tang Y, Wallace M, Sanchez-Gurmaches J, et al. Adipose tissue mTORC2 regulates ChREBP-driven de novo lipogenesis and hepatic glucose metabolism. Nat Commun 2016;7:11365
4. Yilmaz M, Claiborn KC, Hotamisligil GS. De novo lipogenesis products and endogenous lipokines. Diabetes 2016;65:1800–1807
5. Cao H, Gerhold K, Mayers JR, Wiest MM, Watkins SM, Hotamisligil GS. Identification of a lipokine, a lipid hormone linking adipose tissue to systemic metabolism. Cell 2008;134:933–944
6. Flachs P, Adamcova K, Zouhar P, et al. Induction of lipogenesis in white fat during cold exposure in mice: link to lean phenotype. Int J Obes 2017;41:372–380
7. Herman MA, Peroni OD, Villoria J, et al. A novel ChREBP isoform in adipose tissue regulates systemic glucose metabolism. Nature 2012;484:333–338
8. Yore MM, Syed I, Moraes-Vieira PM, et al. Discovery of a class of endogenous mammalian lipids with anti-diabetic and anti-inflammatory effects. Cell 2014;159:318–332
9. Lodhi IJ, Yin L, Jensen-Urstad AP, et al. Inhibiting adipose tissue lipogenesis reprograms thermogenesis and PPARγ activation to decrease diet-induced obesity. Cell Metab 2012;16:189–201
10. Kuda O, Brezinova M, Rombaldova M, et al. Docosahexaenoic acid-derived fatty acid esters of hydroxy fatty acids (FAHFAs) with anti-inflammatory properties. Diabetes 2016;65:2580–2590
11. Zhu QF, Yan JW, Zhang TY, Xiao HM, Feng YQ. Comprehensive screening and identification of fatty acid esters of hydroxy fatty acids in plant tissues by chemical isotope labeling-assisted liquid chromatography-mass spectrometry. Anal Chem 2018;90:10056–10063
12. Lee J, Moraes-Vieira PM, Castoldi A, et al. Branched fatty acid esters of hydroxy fatty acids (FAHFAs) protect against colitis by regulating gut innate and adaptive immune responses. J Biol Chem 2016;291:22207–22217
13. Brezinova M, Kuda O, Hansikova J, et al. Levels of palmitic acid ester of hydroxystearic acid (PAHSA) are reduced in the breast milk of obese mothers. Biochim Biophys Acta Mol Cell Biol Lipids 2018;1863:126–131
14. Schreiber R, Diwoky C, Schoiswohl G, et al. Cold-induced thermogenesis depends on ATGL-mediated lipolysis in cardiac muscle, but not brown adipose tissue. Cell Metab 2017;26:753–763.e7
15. Balas L, Bertrand-Michel J, Viars F, et al. Regiocontrolled syntheses of FAHFAs and LC-MS/MS differentiation of regioisomers. Org Biomol Chem 2016;14:9012–9020

16. Yang D, Diraison F, Beylot M, et al. Assay of low deuterium enrichment of water by isotopic exchange with [U-13C3]acetone and gas chromatography-mass spectrometry. Anal Biochem 1998;258:315–321

17. Cajka T, Smilowitz JT, Fiehn O. Validating quantitative untargeted lipidomics across nine liquid chromatography-high-resolution mass spectrometry platforms. Anal Chem 2017;89:12360–12368

18. Kuda O, Brezinova M, Silhavy J, et al. Nrf2-mediated antioxidant defense and peroxiredoxin 6 are linked to biosynthesis of palmitic acid ester of 9-hydroxystearic acid. Diabetes 2018;67:1190–1199

19. Oseeva M, Paluchova V, Zacek P, et al. Omega-3 index in the Czech Republic: no difference between urban and rural populations. Chem Phys Lipids 2019;220:23–27

20. Lee WN, Bassilian S, Guo Z, et al. Measurement of fractional lipid synthesis using deuterated water (2H2O) and mass isotopomer analysis. Am J Physiol 1994; 266:E372–E383

21. Zhang Z, Chen L, Liu L, Su X, Rabinowitz JD. Chemical basis for deuterium labeling of fat and NADPH. J Am Chem Soc 2017;139:14368–14371

22. Tsugawa H, Cajka T, Kind T, et al. MS-DIAL: data-independent MS/MS de-convolution for comprehensive metabolome analysis. Nat Methods 2015;12:523–526

23. Millard P, Letisse F, Sokol S, Portais JC. IsoCor: correcting MS data in isotope labeling experiments. Bioinformatics 2012;28:1294–1296

24. Previs SF, Herath K, Nawrocki AR, et al. Using [²H]water to quantify the contribution of de novo palmitate synthesis in plasma: enabling back-to-back studies. Am J Physiol Endocrinol Metab 2018;315:E63–E71

25. Krycer JR, Yugi K, Hirayama A, et al. Dynamic metabolomics reveals that insulin primes the adipocyte for glucose metabolism. Cell Rep 2017;21:3536–3547

26. Kuda O. On the complexity of PAHSA research. Cell Metab 2018;28:541–542

27. Syed I, Lee J, Peroni OD, et al. Methodological issues in studying PAHSA biology: masking PAHSA effects. Cell Metab 2018;28:543–546

28. Loos M, Gerber C, Corona F, Hollender J, Singer H. Accelerated isotope fine structure calculation using pruned transition trees. Anal Chem 2015;87:5738–5744

29. Mottillo EP, Balasubramanian P, Lee YH, Weng C, Kershaw EE, Granneman JG. Coupling of lipolysis and de novo lipogenesis in brown, beige, and white adipose tissues during chronic β3-adrenergic receptor activation. J Lipid Res 2014;55:2276–2286

30. McLean S, Davies NW, Nichols DS, Mcleod BJ. Triacylglycerol estolides, a new class of mammalian lipids, in the paracloacal gland of the brushtail possum (Trichosurus vulpecula). Lipids 2015;50:591–604

31. Tan D, Ertunc ME, Konduri S, et al. Discovery of FAHFA-containing tri-acylglycerols and their metabolic regulation. J Am Chem Soc 2019;141:8798–8806

32. Mayer N, Schweiger M, Romauch M, et al. Development of small-molecule inhibitors targeting adipose triglyceride lipase. Nat Chem Biol 2013;9: 785–787

33. Previs SF, McLaren DG, Wang SP, et al. New methodologies for studying lipid synthesis and turnover: looking backwards to enable moving forwards. Biochim Biophys Acta 2014;1842:402–413

34. Zhou P, Santoro A, Peroni OD, et al. PAHSAs enhance hepatic and systemic insulin sensitivity through direct and indirect mechanisms. J Clin Invest 2019;129: 4138–4150

35. Yoo H, Antoniewicz MR, Stephanopoulos G, Kelleher JK. Quantifying re-ductive carboxylation flux of glutamine to lipid in a brown adipocyte cell line. J Biol Chem 2008;283:20621–20627

36. Masoodi M, Kuda O, Rossmeisl M, Flachs P, Kopecky J. Lipid signaling in adipose tissue: connecting inflammation & metabolism. Biochim Biophys Acta 2015;1851:503–518

37. Syed I, Lee J, Moraes-Vieira PM, et al. Palmitic acid hydroxystearic acids activate GPR40, which is involved in their beneficial effects on glucose ho-meostasis. Cell Metab 2018;27:419–427.e4

38. Lake AC, Sun Y, Li JL, et al. Expression, regulation, and triglyceride hydrolase activity of Adiponutrin family members. J Lipid Res 2005;46:2477–2487

39. Jenkins CM, Mancuso DJ, Yan W, Sims HF, Gibson B, Gross RW. Identifi-cation, cloning, expression, and purification of three novel human calcium-independent phospholipase A2 family members possessing triacylglycerol lipase and acylglycerol transacylase activities. J Biol Chem 2004;279:48968–48975

40. Hammarstedt A, Syed I, Vijayakumar A, et al. Adipose tissue dysfunction is associated with low levels of the novel Palmitic Acid Hydroxystearic Acids. Sci Rep 2018;8:15757